BBA - Bioenergetics 1861 (2020) 148206

Contents lists available at ScienceDirect

BBA - Bioenergetics

journal homepage: www.elsevier.com/locate/bbabio

Harvesting far-red light: Functional integration of chlorophyll *f* into Photosystem I complexes of *Synechococcus* sp. PCC 7002

Martijn Tros[a], Luca Bersanini[a], Gaozhong Shen[b], Ming-Yang Ho[b,c], Ivo H.M. van Stokkum[a], Donald A. Bryant[b,d], Roberta Croce[a,*]

[a] Department of Physics and Astronomy and LaserLaB, Faculty of Science, Vrije Universiteit Amsterdam, De Boelelaan 1081, 1081 HV Amsterdam, the Netherlands
[b] Department of Biochemistry and Molecular Biology, The Pennsylvania State University, University Park, PA 16802, USA
[c] Department of Life Science, National Taiwan University, Taipei 10617, Taiwan
[d] Department of Chemistry and Biochemistry, Montana State University, Bozeman, MT 59717, USA

ARTICLE INFO

Keywords:
Photosynthesis
Light harvesting
Pigments
Time-resolved fluorescence
Excitation energy transfer

ABSTRACT

The heterologous expression of the far-red absorbing chlorophyll (Chl) *f* in organisms that do not synthesize this pigment has been suggested as a viable solution to expand the solar spectrum that drives oxygenic photosynthesis. In this study, we investigate the functional binding of Chl *f* to the Photosystem I (PSI) of the cyanobacterium *Synechococcus* 7002, which has been engineered to express the Chl *f* synthase gene. By optimizing growth light conditions, one-to-four Chl *f* pigments were found in the complexes. By using a range of spectroscopic techniques, isolated PSI trimeric complexes were investigated to determine how the insertion of Chl *f* affects excitation energy transfer and trapping efficiency. The results show that the Chls *f* are functionally connected to the reaction center of the PSI complex and their presence does not change the overall pigment organization of the complex. Chl *f* substitutes Chl *a* (but not the Chl *a* red forms) while maintaining efficient energy transfer within the PSI complex. At the same time, the introduction of Chl *f* extends the photosynthetically active radiation of the new hybrid PSI complexes up to 750 nm, which is advantageous in far-red light enriched environments. These conclusions provide insights to engineer the photosynthetic machinery of crops to include Chl *f* and therefore increase the light-harvesting capability of photosynthesis.

1. Introduction

Photosystem I (PSI) is a light-driven plastocyanin/cytochrome c_6: ferredoxin/flavodoxin oxidoreductase composed of eleven or twelve polypeptides [1,2]. The PSI core complex binds 95 chlorophyll (Chl) *a* molecules, 22 β-carotenes, 2 phylloquinones (or menaquinone-4), and three [4Fe−4S] clusters [3–7]. The Chls are exclusively Chl *a* in algal, plant and most cyanobacterial PSI core complexes [5,8]; 89 Chl *a* molecules form the core antenna, while the additional six participate in the electron transport chain. PSI is remarkably efficient in converting light energy into stored chemical potential energy, with an overall quantum efficiency close to 100% [9–12]. PSI possesses photochemically active pigments absorbing at 700 nm. This wavelength has for a long time represented the “red limit” of oxygenic photosynthesis, meaning the minimal energy required to support photochemical oxidation of water [9,13–15]. However, it was found that the cyanobacterium *Acaryochloris* extends this limit by using Chl *d* [16], a pigment absorbing at 30 nm longer wavelengths than Chl *a* [17,18]. More recently, Chl *f*, the longest-wavelength chlorophyll known (max Q_y = 706 nm in organic solvents) [19,20], and the enzyme responsible for its synthesis from Chl *a* or Chlide *a* (Chl *f* synthase [21]) were discovered. Chl *f* is produced by some terrestrial cyanobacteria when they grow in environments enriched in far-red light (FRL) (λ = 700–800 nm [22]) such as soils, rocks, caves, microbial mats, and under the shade of plants. These organisms are able to perform Far-Red Light Photoacclimation (FaRLiP) [22–24], which involves the synthesis of Chl *d* and *f*, in addition to the common Chl *a*, and substitution of pigment-binding subunits with products of gene variants from a 21-gene cluster [22,24]. These

Abbreviations: CS, charge separation; Chl, chlorophyll; CD, Circular Dichroism; DAS, decay-associated spectra; EAS, evolution associated spectra; EET, excited energy transfer; ETC, electron transport chain; FaRLiP, far-red light photoacclimation; FRL, far-red light; FWHM, full-width at half max; GL, green light; HPLC, high performance liquid chromatography; IRF, instrument response function; LL, low-intensity white light; PAR, photosynthetically active radiation; PSI, Photosystem I; PSII, Photosystem II; RC, reaction center; RT, room temperature; SAS, species associated spectra; WT, wild type; WL, cool-white fluorescent light

* Corresponding author.
E-mail address: r.croce@vu.nl (R. Croce).

https://doi.org/10.1016/j.bbabio.2020.148206
Received 22 January 2020; Received in revised form 1 April 2020; Accepted 14 April 2020
Available online 17 April 2020

combined changes lead to extensive remodeling of the photosynthetic apparatus and allow FaRLiP organisms to perform oxygenic photosynthesis using FRL. In fact, PSI and PSII gain absorbance up to 800 nm due to the presence of Chls *d* and *f* associated with paralogous PSI and PSII subunits [7,23,25]. Recent studies have shown that Chl *f* is associated with both FRL-PSI (8%) and FRL-PSII (11.4–12.7%), while Chl *d* is exclusively associated with FRL-PSII (2.9–4%) [25,26].

The discovery of Chl *d* and Chl *f* in cyanobacteria [16,19,27,28], and in particular of a Chl *f* synthase enzyme [21], has opened the way to the production of these pigments in algae or higher plants, with the potential to enhance photosynthetic efficiency and crop productivity. It was estimated that by expressing Chl *f*, the photosynthetically active radiation (PAR) could be expanded into the FRL region [12,21], increasing the number of available photons by 19% when extended to 750 nm [29,30]. The suggested approach, following a smart canopy concept [31], could increase the light-harvesting capacity in the lower leaves of the canopy or at the bottom of a pond/bioreactor, that mainly receive light enriched in far-red wavelengths [29,31–33]. The expansion of the photosynthetically active radiation could also provide an advantage in non-saturating light conditions. Recent evidence demonstrated that the efficiency of photosynthetic energy storage in a cyanobacterium producing red-shifted Chls is comparable or higher than that in Chl *a*-containing species [34]. However, whether photosynthesis would be efficient in genetically engineered organisms expressing Chl *d* or *f*, in combination with their WT photosynthetic proteins is still an open question. Recently, the Chl *f* synthase was successfully expressed in the non-FaRLiP cyanobacterium *Synechococcus* sp. PCC 7002 (hereafter Synechococcus 7002) [21,35]. Depending on the growth light conditions, the PSI of strains expressing the *chlF* gene accommodate a different number of Chl *f* pigments depending upon strain background and growth conditions [35]. In this work, by means of time-resolved fluorescence spectroscopy, we quantitatively investigated how the inserted Chls *f* are functionally connected to the bulk Chl within PSI and how their presence influences the quantum efficiency of PSI.

2. Materials and methods

2.1. Strains and growth conditions

Synechococcus sp. PCC 7002 (hereafter *Synechococcus* 7002) wild type (WT) and the engineered strain WT::*ChlF* with heterologous expression of the *chlF* gene of *Fischerella thermalis* PCC 7521 (hereafter Ft7521 [35]) were grown in liquid A^+ medium under standard conditions as previously described: 250 μmol photons m^{-2} s^{-1} cool-white fluorescent light (WL), 38 °C, and sparging with 1% (v/v) CO_2 in air [36]. The ΔPSII::*ChlF* mutant, obtained by deleting the *psbD1* and *psbD2* genes but expressing the *chlF* gene from Ft7521 [35], was grown under different light qualities: low-intensity white light (LL: ~10 μmol photons m^{-2} s^{-1}), green light (GL: 11 μmol photons m^{-2} s^{-1}) and FRL (25–30 μmol photos m^{-2} s^{-1}) and the medium was supplemented with 20 mM glycerol [37]. Differences in light qualities were obtained with neutral density filters as described previously [22,23].

2.2. Purification of trimeric Photosystem I complexes

PSI complexes were purified from WT, WT::*ChlF*, ΔPSII::*ChlF* cells grown at different light conditions by sucrose gradient centrifugation of membrane solubilized proteins, following procedures described previously [35,38,39]. Purified PSI complexes were resuspended in MES buffer (pH 6.5) containing 10 mM $CaCl_2$, 10 mM $MgCl_2$, 0.05% (w/v) β-D-dodecyl maltoside (DM) and 5% (w/v) glycerol.

2.3. Pigment extraction and analysis

Cyanobacterial cells were harvested by centrifugation and washed once in 50 mM HEPES pH 7.2 prior to pigment extraction and analysis. Pigments were extracted from purified PSI complexes and analyzed by procedures described in Shen et al. [35]. The HPLC data were processed using Agilent ChemStation software (revision B.02.01-SR1 6100 series). The number of Chl *f* molecules per PSI complex was calculated from the % composition of Chl *a* and *f* in the complexes as determined by reversed-phase HPLC analysis and by assuming that a PSI monomer contains 95 total Chl molecules [7,40].

2.4. Absorption, Circular Dichroism and steady state fluorescence measurements

Room temperature (RT) absorption spectra of isolated PSI complexes were recorded with a Cary 4000 spectrophotometer (Agilent Technologies, Santa Clara, CA United States). The Circular Dichroism (CD) spectra were measured using a Chirascan CD Spectrophotometer (Applied Photophysics, Leatherhead, United Kingdom) with samples at OD 0.5 at the maximum of the Qy absorption band. The buffer conditions of the samples were kept the same as the stock solutions of the purified PSI complexes, i.e. in 50 mM MES buffer (pH 6.5) containing 10 mM $CaCl_2$, 10 mM $MgCl_2$, 0.05% (w/v) β-DM and 5% (w/v) glycerol. The fluorescence emission spectra were recorded at 77 K and RT using a Fluorolog 3.22 spectrofluorimeter (Jobin Yvon-Spex, Longjumeau, France). The excitation wavelength was 500 nm and emission was detected in the 600–850 nm range. Excitation and emission bandwidths were set to 3 nm. All fluorescence spectra were measured at OD 0.05 at the maximum of the Q_y absorption band. For 77 K measurements a liquid nitrogen cooled device was used (Nitrogen Cold finger).

2.5. Time-resolved fluorescence measurement

Time-resolved fluorescence decays of isolated PSI complexes were recorded with a Hamamatsu C5680 synchroscan streak camera, combined with a Chromex 250IS spectrograph. A grating of 50 grooves per mm and blazed wavelength of 600 nm was used. The central wavelength was set at 720 nm, giving a detection range from 590 nm to 860 nm and a time range from 0 to 350 ps (TR2 temporal response of 5–6 ps) was chosen. The 400 nm excitation light was vertically polarized, the spot size diameter was typically ~100 μm, and the laser repetition rate was 250 kHz [41]. The laser power was set to 200 μW, after a careful power-dependent study confirmed the absence of annihilation in these conditions (see power-dependent studies in Supplemental Fig. S2). Approximately 500 μL sample with optical density of 0.5 at the maximum of the Q_y absorption band was measured at RT. The sample was magnetically stirred in a cuvette with speed of 750 rpm and to avoid reabsorption the excitation laser was focused in the sample close to the cuvette walls. The averaged image was corrected for background and shading, and then sliced into traces of ~2 nm width.

2.6. Global and target data analysis

Data obtained with the streak-camera setup were first globally analyzed with the R package TIMP-based Glotaran [42]. The methodology of global analysis is described in [43,44]. The datasets were analyzed with a sequential model, the evolution associated spectra (EAS) from the resulting analysis were used to calculate the decay associated spectra (DAS). The instrument response function (IRF) was fitted with a single Gaussian with a full width at half max (FWHM) of 5–6 ps. The amplitudes of the resulting DAS are normalized to the first EAS, which is the t_0 spectrum. Disregarding the longest lifetime which is attributed to free pigments, the average decay lifetimes τ_{avg} could be calculated from the sum of all lifetimes weighed by the relative amplitudes of each of the DASs: $\tau_{avg} = \Sigma(\tau_n * A_n) / \Sigma(A_n)$. In which A_n is the amplitude calculated as the area under the DAS of component *n* and τ_n its respective decay lifetime. This average lifetime, representing the time in which charge separation (CS) occurs, can be used to calculate

the efficiency of the PSI complex. This quantum efficiency of CS, Φ_{CS}, is calculated with $\Phi_{CS} = 1-(\tau_{avg} / \tau_{noCS})$ where τ_{noCS} is the decay time of the excitation when no CS occurs. For τ_{noCS} the natural fluorescence decay rate of free Chl *a* (0.2 ns^{-1}) is used.

In a target analysis the datasets of all five samples were simultaneously fitted with the same kinetic model (Fig. 3A). In this model the PSI core complexes were described with three compartments for respectively the bulk Chl *a*, red Chl *a* and the newly introduced Chl *f* pigments. Additionally, two compartments had to be added to account for the small but variable amounts of free Chl *a* and free Chl *f* with ns-lifetime emission. For the PSI0-Chlf sample, which did not contain Chl *f*, the bound and free Chl *f* compartments were removed in the analysis. As 400 nm excitation light was used all compartments are populated from the Soret compartment (see Supplemental Methods S1 for more details).

3. Results

3.1. Integration of Chl f into the native PSI protein of Synechococcus 7002

Like the majority of cyanobacteria, also Synechococcus 7002 synthesizes only Chl *a*, which is incorporated into PSI and PSII. The Chl *f* synthase gene (*ChlF*) from *Fischerella thermalis* PCC 7521 was heterologously expressed in Synechococcus 7002 WT and ΔPSII strains, as previously described [21,35]. The resulting strains, designated WT::*ChlF* and ΔPSII::*ChlF*, respectively, were grown at different light intensities and using different light colours (white, green, far-red) [35]. From these strains, the PSI trimeric complexes were isolated by sucrose density gradients and subsequently analyzed with different techniques. The properties of these complexes were compared with those of PSI trimers purified from the WT Synechococcus 7002 strain.

HPLC analysis of PSI pigment extracts showed that Chl *f* was bound to the PSI complexes (Table 1). However, the content of Chl *f* per PSI varied according to the different growth light conditions, from a minimum of ~1 Chl *f* per PSI (WT::*ChlF* in WL) to a maximum of ~4 Chl *f* per PSI (ΔPSII::*ChlF* in FRL) [12,35].

Absorption spectra of isolated PSI complexes containing Chl *f* revealed a long-wavelength shoulder when compared to WT PSI (Fig. 1A). The shoulder increased in intensity as the content of Chl *f* per PSI increased (Fig. 1A insert). Similarly, at room temperature (RT) the fluorescence emission at 720 nm (Fig. 1B) increased with the number of Chl *f* per complex, and at 77 K the emission band gradually shifted from 714 nm for PSI-0Chlf to 719 nm for PSI-4Chlf (Fig. S1). The CD spectra of these complexes were not significantly different from those of the WT (Fig. 1C), which suggested that no major changes in the overall pigment organization had occurred to accommodate the Chl *f* molecules.

3.2. Excitation energy transfer and trapping in PSI-Chl f-containing complexes

Time-resolved fluorescence measurements with excitation at 400 nm were performed on the PSI complexes with a streak camera setup, and the data were globally analyzed. The kinetics of all the PSI complexes isolated from different strains/growth conditions could be well-fitted with four components. In Fig. 2 and Table 2 respectively, the

Table 1
Strains, growth conditions and calculated Chl *f* amounts per PSI monomeric complex quantified from HPLC analysis.

Name of the strain	Growth conditions	# of Chl *f* per PS I	Short name
WT	White light (WL)	0 (0%)	PSI-0Chlf
WT::*ChlF*	White light (WL)	1.1 (1.1%)	PSI-1Chlf
ΔPSII::*ChlF*	Low light (LL)	1.6 (1.7%)	PSI-1.5Chlf
	Green light (GL)	2.6 (2.7%)	PSI-2.5Chlf
	Far-red light (FRL)	3.8 (4.0%)	PSI-4Chlf

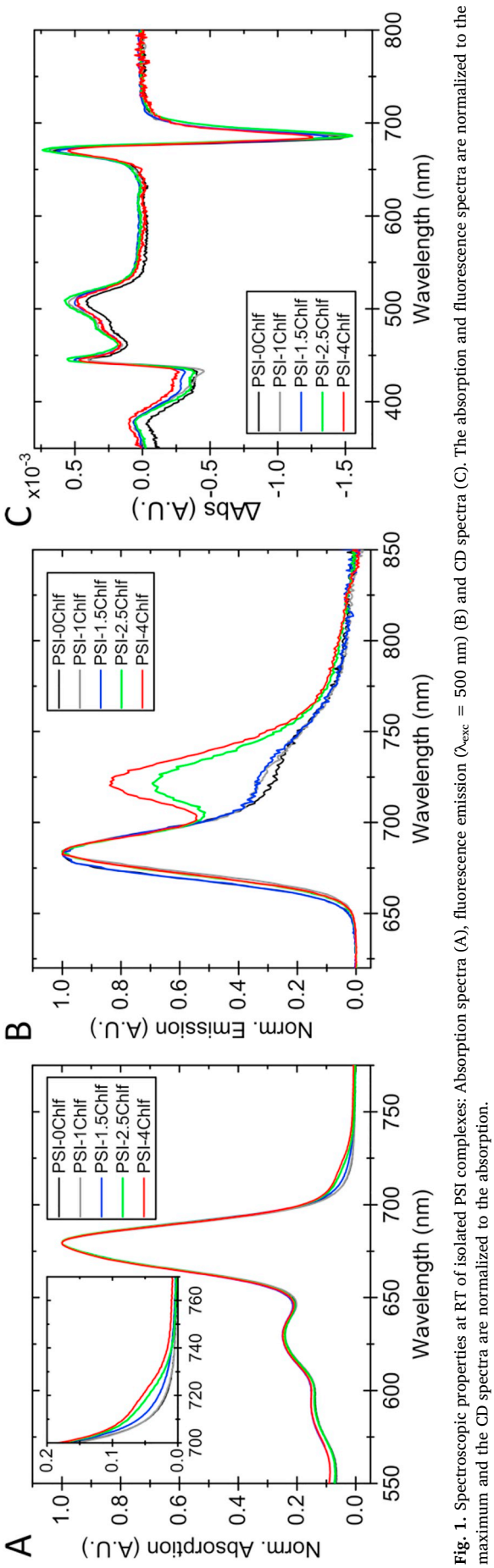

Fig. 1. Spectroscopic properties at RT of isolated PSI complexes: Absorption spectra (A), fluorescence emission (λ_{exc} = 500 nm) (B) and CD spectra (C). The absorption and fluorescence spectra are normalized to the maximum and the CD spectra are normalized to the absorption.

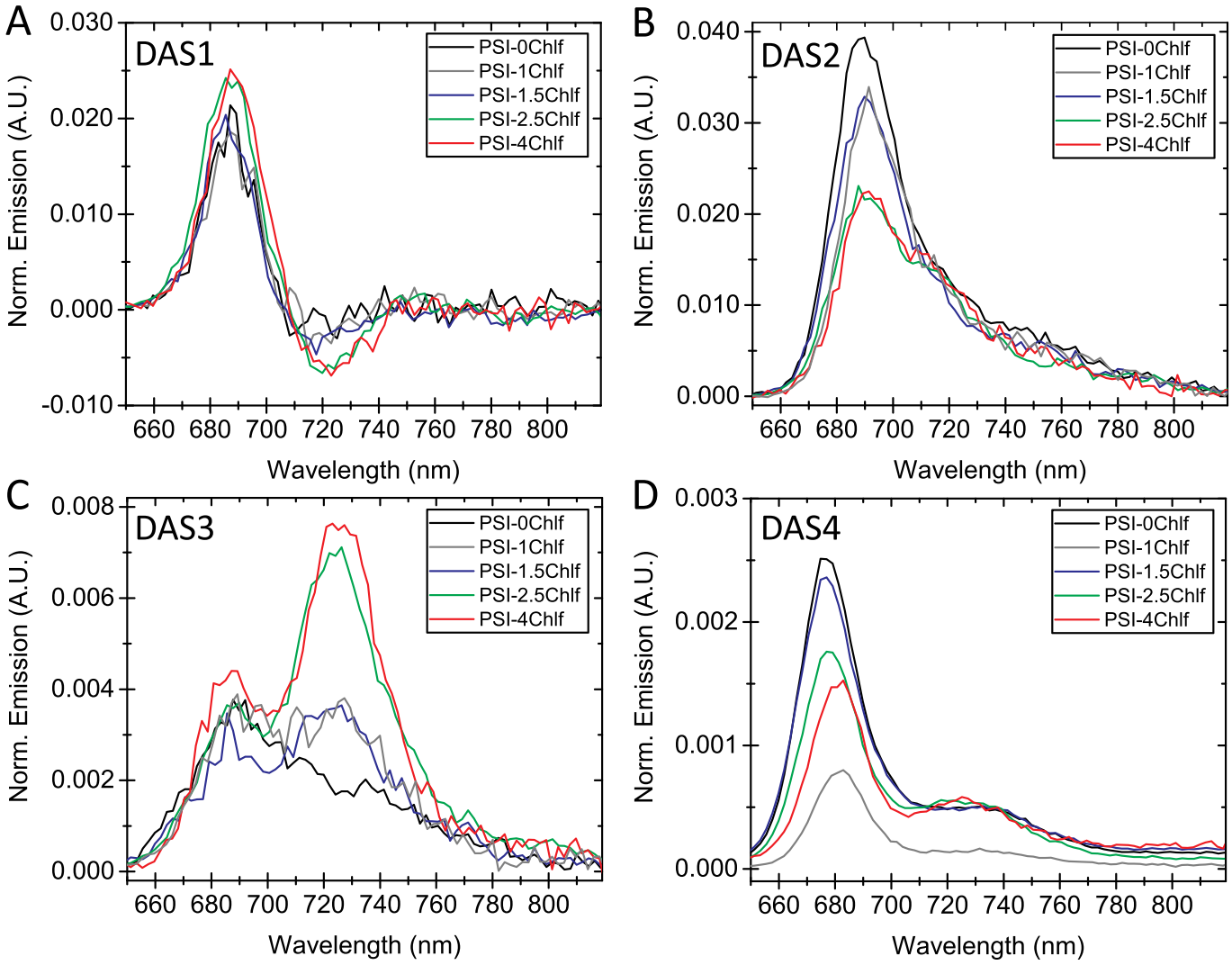

Fig. 2. Decay Associated Spectra (DAS) obtained from time-resolved fluorescence emission measurements performed at RT upon 400 nm excitation on the PSI samples normalized to the T_0 spectrum of each sample.

decay associated spectra (DAS) and corresponding lifetimes of the PSI samples are displayed.

The first component (Fig. 2A) with a lifetime of 4–6 ps represents excitation energy transfer (EET) from bulk Chls *a* to red Chls *a* and *f* (when present). The red-shifted bleach in the spectra of PSI-2.5Chlf and PSI-4Chlf compared to the other samples can be assigned to Chl *f*, the content of which is higher in these complexes. The second component (16–19 ps) is dominated by the decay; it accounts for most of the trapping and has a similar lifetime in the five complexes. A small but significant broadening of DAS2 is observed in the samples with higher Chl *f* content (Fig. 2B), especially in the spectra of the PSI-2.5Chlf and PSI-4Chlf samples. Similar to DAS2, DAS3 (Fig. 2C) of WT PSI (PSI-0Chlf) has a maximum at 690 nm. However, a broad shoulder is present in the far-red region, which can be assigned to red-shifted Chls *a* [11,45]. The insertion of Chl *f* in PSI results in a significant change of DAS3: PSI-1Chlf and PSI-1.5Chlf show a new peak at $\lambda = 721$ nm (grey and blue traces in Fig. 2C), the relative amplitude of which increases in the samples with 2.5 Chl *f* and 4 Chl *f* per PSI (green and red traces in Fig. 2). The DAS3 lifetime increases only slightly at increasing Chl *f* content (from 40 to 60 ps, see Table 2), indicating that the Chls *f* molecules are very well connected to the reaction center (RC) and that trapping still occurs very efficiently.

DAS4 (Fig. 2D) has a very small amplitude and a lifetime of about 4 ns for all samples (Table 2). It represents the contribution of

Table 2
Results from global analysis. Each dataset is normalized to the T_0 spectrum. The average lifetimes τ_{avg} were calculated (disregarding the longest lifetime) with the formula $\tau_{avg} = \Sigma(\tau_n * A_n) / \Sigma(A_n)$. The quantum efficiency of charge separation (CS) Φ_{CS} was calculated with $\Phi_{CS} = 1-(\tau_{avg} / \tau_{noCS})$ where τ_{noCS} is the free Chl *a* decay rate of 0.2 ns^{-1}.

Sample	A1 (%)	τ_1 (ps)	A2 (%)	τ_2 (ps)	A3 (%)	τ_3 (ps)	A4 (%)	τ_4 (ns)	τ_{avg} (ps)	Φ_{CS} (%)
PSI-0Chlf	20.3	4.5	58.1	16.5	17.6	35.2	4.0	4.74	17.4	99.7
PSI-1Chlf	18.3	5.7	66.8	18.1	13.6	42.4	1.4	6.09	19.1	99.6
PSI-1.5Chlf	14.8	5.2	68.0	18.9	12.4	47.1	4.8	3.84	20.4	99.6
PSI-2.5Chlf	21.7	5.9	54.8	18.6	19.7	61.0	3.8	4.46	24.4	99.5
PSI-4Chlf	20.7	5.0	54.	17.7	20.9	59.6	3.7	4.91	24.1	99.5

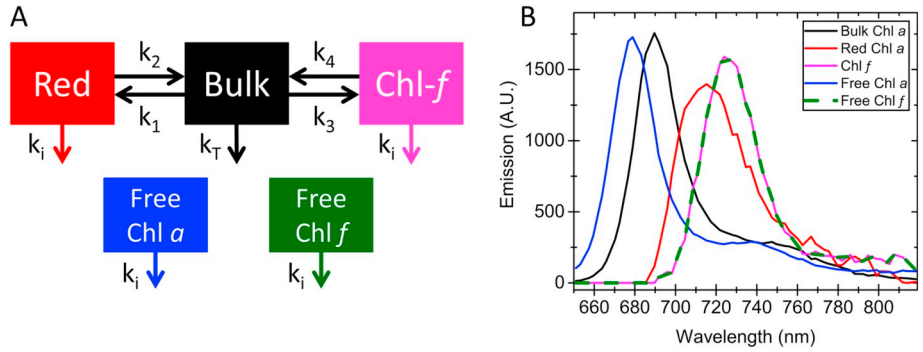

Fig. 3. Model used for the simultaneous target analysis of all datasets from Chl *f*-containing PSI samples (A). The full model is shown in Supplemental information (Fig. S3). Estimated SAS of Bulk Chl *a*, Red Chl *a*, Chl *f* and free Chls *a* and *f* (B).

disconnected Chls *a* (max at ~680 nm) and possibly Chl *f* (max at ~720 nm).

The presence of Chl *f* in the PSI complexes results in an increased average lifetime τ_{avg} (Table 2) in all samples with the exception of PSI-4Chlf. Despite the increase of τ_{avg}, in all samples, the trapping is still very fast in comparison to the intrinsic decay kinetics of the pigments, and thus the quantum efficiency of CS Φ_{CS} (Table 2) remains high.

3.3. Target analysis

To understand better how the insertion of Chl *f* influences excitation energy transfer and trapping kinetics within the new hybrid PSI complexes, all datasets were simultaneously subjected to a target analysis.

The kinetic model was based on the isolated PSI core model [41,46,47], consisting of two compartments to describe the bulk and red Chls *a* (respectively, black and red boxes in Fig. 3A). An extra compartment was included in the model to account for a small amount of disconnected/free Chl *a* pigments (blue box in Fig. 3A). These three compartments were used to describe the PSI-0Chlf sample. As in the global analysis the maximum of DAS3 is at the same position as in DAS2 and its intensity is relatively small, only one compartment was used for the red Chls *a*. For the PSI complexes containing Chl *f*, two additional compartments were required: one representing Chl *f* connected to the bulk Chl *a* compartment and a second one representing the small amount of free Chl *f* (respectively, magenta and green boxes in Fig. 3A), observed in the global analysis. Trapping was only allowed to occur from the bulk compartment and, as it was assumed that no Chl *f* was inserted in the RC, the trapping rate k_T was set to be equal for all samples. The decay rates of the PSI red and the free Chl *f* compartments were set to be equal to the intrinsic decay rate of free Chl *a* $k_i = 0.2\ ns^{-1}$ because the excited state lifetime of Chl *f* in solvents is very similar to that of Chl *a* [48]. The amplitudes of the Species Associated Spectra (SAS) for the red and the Chl *f* compartments were set to zero below 685 nm and 690 nm, respectively. Equal area constraints for the area under each SAS were applied and the spectrum of free Chl *f* was assumed to be equal to the SAS of Chl *f* within the complex. The area of the Chl *f* SAS is expected to be very similar to the one of Chl *a*, because the extinction coefficients of the two Chls were found to be almost the same [49]. Although the position of Chl *f* emission band (721 nm) is very close to that of the pigment in solvent (Pyridine [48]), we cannot exclude the possibility that the spectrum of Chl *f* bound to the protein differs from that of the pigment in the buffer solution. However, as the concentration of free Chl *f* is very low and its fluorescence decay is much longer than the energy trapping in the PSI RC, it will not have a large effect on the calculations. Moreover, the free Chl *f* signal observed in DAS4 of the global analysis (Fig. 2D) peaks at a comparable position with the bound Chl *f* (Figs. 2C, 1B). In the fit it was assumed that the insertion of Chl *f* did not affect the red Chl *a* forms, i.e. the energy transfer rates k_1 and k_2 between the bulk and red compartments were assumed to be equal among the samples. Only for the PSI-4Chlf sample these rates had to be adapted slightly. This assumption is supported by the Chl *f* emission bands at $\lambda = 721$ nm in the steady-state emission spectra (Fig. 1B) and DAS3 from the global analysis (Fig. 2C). The increasing amplitude of this band indicates the integration of a different number of Chl *f* molecules in the complexes. However, the central wavelength of the band is independent on the number of integrated Chl *f*, indicating a similar environment of all inserted Chls *f*. Moreover, this central wavelength is very similar to that of Chl *f* in solvent (Pyridine [48]). If a Chl *f* would replace one of the red Chls *a* the strong interaction between Chls is expected to result in a significantly more red shifted band (> 720 nm). Although the fractional binding stoichiometry of PSI-1.5Chlf and PSI-2.5Chlf indicate that these samples contain heterogeneous populations of complexes with different amounts of Chl *f*, they can still be described with a homogeneous kinetic model as the physiochemical environment of the integrated Chls *f* is very similar.

As demonstrated in Fig. S4, this kinetic model fits the datasets very well, and the additional emission attributable to Chl *f* is well visible. The estimated SAS resulting from the simultaneous fit of all the samples are displayed in Fig. 3B and the estimated kinetic rates are listed in Table S1. The decay rate of the bulk compartment from which CS occurs was estimated to be $k_T = 64\ ns^{-1}$, which is similar to the trapping rates reported before for isolated PSI [46,47,50,51]. The first SAS (black) represents the spectrum of the bulk Chl *a*, peaking at 690 nm. The SAS for the Red Chl *a* (red) and Chl *f* (pink) compartments are well separated. The SAS of the Red compartment is centered at 715 nm, which is in agreement with the emission of the most red-forms of *Synechococcus* 7002 [52]. The spectrum is also broader than that of the other compartments, which is a typical property of the spectra of the far-red forms [47,51,52]. The emission spectrum of the Chl *f* (pink) compartment peaks at 723 nm, which matches the wavelength of the red band seen in the RT emission spectra of PSI-2.5Chlf and PSI-4Chlf (Fig. 1B). The increasing Chl *f* content results in an increase in the energy transfer rates k_3 and k_4 between the bulk and Chl *f* compartments (Table S1) with the equilibrium shifting to the latter one. The free Chl *a* SAS (blue) peaks at 678 nm with a distinct long vibrational band in the red. The amounts of free Chls *a* and *f* in all samples are listed in Table S2 (see Supplemental Methods S1 for more details).

The time dependence of the concentrations of each compartment for the different samples is given by the amplitude matrices, which are displayed in Table 3. The matrix shows the lifetime and corresponding amplitudes of the population (negative amplitude) and depopulation/decay (positive amplitude) of each compartment [41,51,53]. When focusing on the Red and Chl *f* compartments, it is seen that in all samples the first lifetime component of around 7 ps represents energy transfer from bulk to red Chls and a minor portion of the Chl *f*. The second component of 15–20 ps encompasses two major events, namely i) trapping of the energy from the Red compartment and ii) population

Table 3
Amplitude matrices of all samples calculated from results target analysis.

Sample	τ (ps)	Amplitude compartment			Trapped slowly
		Red	Chl *f*	Bulk Chl	
PSI-0Chlf	7.18	−0.204	–	0.375	
	20.8	0.199	–	0.593	
	–	–	–	–	0%
PSI-1Chlf	7.14	−0.210	−0.005	0.396	
	20.1	0.201	−0.031	0.583	
	46.4	0.005	0.036	0.020	3.5%
PSI-1.5Chlf	7.07	−0.205	−0.015	0.401	
	17.1	0.122	−0.095	0.296	
	26.2	0.078	0.110	0.274	10.8%
PSI-2.5Chlf	6.90	−0.207	−0.041	0.445	
	16.7	0.177	−0.147	0.417	
	44.2	0.027	0.186	0.115	18.2%
PSI-4Chlf	4.55	−0.211	−0.023	0.329	
	15.1	0.174	−0.191	0.523	
	44.7	0.030	0.211	0.128	21.5%

of the Chl *f* from the bulk. This energy, and the remaining energy from the red Chls, is trapped in ~45 ps (third component). As expected the amplitudes of the Chl *f* compartment increase with the increase in Chl *f* content. Because the trapping time of ~45 ps is still much faster than the natural fluorescence decay time of Chl (5 ns), the depopulation of PSI excited states almost exclusively occurs by charge separation. The percentages of excitation trapped slowly were calculated from these depopulation amplitudes and are listed in Table 3. In contrast to the global analysis, in this target analysis the contribution of the Red Chls *a* and Chls *f* can be resolved and quantified completely. In Table 3, the amplitude of the Chl *f* decay with ≈44 ps differs significantly for PSI-2.5Chlf and PSI-4Chlf, being 0.186 and 0.211, respectively.

4. Discussion

To address how photosynthetic efficiency is affected by the presence of far-red-absorbing chlorophylls in engineered systems, we characterized PSI complexes differing in the number of Chl *f* molecules. In these complexes, a Chl *f* content up to 4% could be reached in optimized growth conditions (Table 1) [35], which represents 50% of the Chl *f* content in the PSI of FaRLiP cyanobacterial strains when they are grown in FRL [24,25]. It should be noted that while in the FaRLiP strains the Chls *f* are associated with paralogs of the PSI subunits only expressed in FR light, in the *Synechococcus* 7002 strains, they are associated with the WT proteins of this model cyanobacterium. The successful integration of Chl *f* into the PSI complexes of this cyanobacterium that normally contain only Chl *a*, under different conditions [35], resulted in hybrid complexes with increased far-red absorption and emission (Fig. 1).

The results presented here show that the Chl *f* pigments are functionally connected to the other pigments in the complexes. As expected, the low-energy states of the Chl *f* pigments function as local traps with a trapping rate that is approximately two and a half times lower than the trapping from the red Chl *a* molecules. As a result, the overall trapping time in the Chl *f*-containing PSI is longer than in the WT complexes, but it is still far shorter than that the intrinsic decay processes of the pigments, assuring a high trapping efficiency (99.5% or greater).

Target analysis supports the view that the presence of Chl *f* does not substitute the far-red Chl *a* forms in any of the samples. In agreement with Kurashov et al. [12], our data also suggest that the Chl *f* pigments in these hybrid PSI-Chlf complexes are not associated with the electron transport chain (ETC) in the RC subdomain: if Chl *f* would be present in the ETC, no Chl *f* fluorescence would be emitted, while Chl *f* emission is observed in all the samples and its intensity increases with the number of Chls *f* associated with the complexes (Figs. 1B-2C).

Notably, the Chls *f* bound to the PSI subunits of *Synechococcus* 7002 are not as red-shifted as the Chls *f* bound to the PSI subunits of FaRLiP cyanobacteria expressed under FRL [23], which extend the absorption region to approximately 800 nm [12,25,35]. However, the addition of a small number of Chls *f* in the *Synechococcus* 7002 PSI complexes with WT sequence still permits to extend the photosynthetically active radiation up to 750 nm. In the complexes analyzed in this work the enhancement in FRL absorption > 700 nm is limited up to 7% of the total Q_Y absorption (λ = 600–750 nm) (Fig. 4A, red). Although this enhancement is rather small, it can have a large effect in FRL-enriched environments. To quantify this effect, we calculated the wavelength distribution of the photons absorbed by the PSI complexes (A_{wl}) at the bottom of a dense plant canopy [22,33] (Fig. 4). The effective absorption of the PSI complexes in this environment is calculated by i) normalizing the absorption spectra of Fig. 1A to their respective area (total Q_Y absorption, range λ = 600–750 nm, Fig. 4A, black and red) and (ii) multiplying these normalized spectra with the irradiance spectrum of the light under the leaf canopy (Fig. 4A, blue). In the resulting spectra (Fig. 4B), showing the light that is absorbed by the PSI complexes under a dense plant canopy, the absorption in the far-red significantly increases with the number of integrated Chl *f*. From these spectra, the share of absorbed far-red photons is calculated by $A_{wl>700nm} = \sum_{700}^{750} A_{wl} / \sum_{600}^{750} A_{wl}$. Similarly, $A_{wl>700nm}$ was calculated for the complexes in unshaded sunlight [22,33] (Fig. 4A, purple). The absorption enhancement due to Chl *f* is quantified by comparing the absorption of the Chl *f*-containing complexes with that of PSI-0Chlf ($R_{Abs} = (\sum_{600}^{750} A_{wl} - \sum_{600}^{750} A_{wl}(\text{PSI-0Chlf})) / \sum_{600}^{750} A_{wl}(\text{PSI-0Chlf})$). The results are shown in Table 4.

Under the shade of a dense plant canopy a significant part of charge separation events would be caused by far-red photons (Fig. 4B), as plants absorb little light > 700 nm [33,54] (Fig. 4A, blue). Here more than half of the red light absorbed by the 4 Chl *f* pigments (3.8%) is FRL (Fig. 4B, Table 4), leading to a 50% increase in total light energy absorption compared to PSI-0Chlf (Table 4). Obviously, increasing the number of Chl *f* molecules by a factor of two and shift their absorption further to the red to achieve the properties typically observed in FRL-PSI complexes of FaRLiP cyanobacteria would produce a much greater impact on photosynthesis by leaves beneath the canopy.

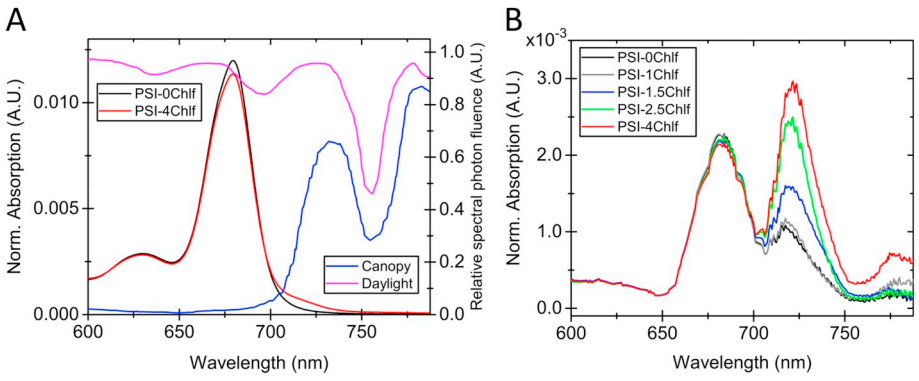

Fig. 4. A) Absorption spectra of PS-0Chlf (black) and PSI-4Chlf (red) normalized to the total Q_Y absorption (λ = 600–750 nm) and relative spectral photon fluence (irradiance) of unshaded sunlight (daylight) and light filtered by a dense leaf canopy (canopy) taken from Gan and Bryant [22]. B) Wavelength distribution A_{wl} of photons absorbed under a dense plant canopy by the PSI complexes.

Table 4
Share $A_{wl > 700nm}$ of absorbed far-red (> 700 nm) photons from the total Q_Y absorption (λ = 600–750 nm) in unshaded sunlight (daylight) and under a dense leaf canopy (canopy). Resulting enhancement R_{Abs} in the total absorption under a dense leaf canopy over the range λ = 600–750 nm compared to the absorption of the PSI-0Chlf complex.

Sample	$A_{wl > 700nm}$ daylight (%)	$A_{wl > 700nm}$ canopy (%)	R_{Abs} canopy (%)
PSI-0Chlf	3.57	32.1	+0
PSI-1Chlf	3.73	34.7	+3.50
PSI-1.5Chlf	4.54	41.3	+14.5
PSI-2.5Chlf	5.47	47.1	+26.2
PSI-4Chlf	6.57	55.9	+48.8

In conclusion, these results, together with those of Kurashov et al. [12] provide positive feedback for enhancing light harvesting in crop plants by extending the solar spectrum for photosynthesis via Chl *f* expression (Chen and Blankenship 2011; Blankenship and Chen 2013). This could be possible by the heterologous expression of only the Chl *f* synthase gene since PSI proteins that have evolved to bind only Chl *a* are nevertheless able to accommodate Chl *f*. However, to achieve optimal FRL utilization, extending the absorption to 800 nm, further and careful engineering of protein subunits of the native photosynthetic complexes would be required. Furthermore, in order to know how the integration of Chl *f* in the photosynthetic apparatus affects the energy uptake and efficiency of the whole photosynthetic process, will be vital to investigate the consequences of Chl *f* insertion on the performance of PSII.

Declaration of competing interest

The authors declare that they have no known competing financial interests or personal relationships that could have appeared to influence the work reported in this paper.

Acknowledgements

This work was supported by the Dutch Organization for Scientific Research via a TOP grant (714.018.001) to R.C. L.B was supported by the EMBO long-term fellowship (EMBO ALTF 292-2017). DAB gratefully acknowledges support from the U. S. National Science Foundation (MCB-1613022). This research was also conducted under the auspices of the Photosynthetic Antenna Research Center (PARC), an Energy Frontier Research Center funded by the DOE, Office of Science, Office of Basic Energy Sciences under Award Number DE-SC 0001035 (DAB).

Appendix A. Supplementary data

Supplementary data to this article can be found online at https://doi.org/10.1016/j.bbabio.2020.148206.

References

[1] N. Nelson, W. Junge, Structure and energy transfer in photosystems of oxygenic photosynthesis, Annu. Rev. Biochem. 84 (2015) 659–683, https://doi.org/10.1146/annurev-biochem-092914-041942.
[2] J.H. Golbeck, D.A. Bryant, Photosystem I, Curr. Top. Bioenerg. 16 (1991) 83–177.
[3] P. Jordan, P. Fromme, H.T. Witt, O. Klukas, W. Saenger, N. Krauss, Three-dimensional structure of cyanobacterial photosystem I at 2.5 A resolution., Nature. 411 (2001) 909–917. doi:https://doi.org/10.1038/35082000.
[4] I. Grotjohann, P. Fromme, Structure of cyanobacterial Photosystem I, Photosynth. Res. 85 (2005) 51–72, https://doi.org/10.1007/s11120-005-1440-4.
[5] R. Croce, R. van Grondelle, H. van Amerongen, I.H.M. van Stokkum, Light Harvesting in Photosynthesis, CRC Press, 2018.
[6] T. Malavath, I. Caspy, S.Y. Netzer-El, D. Klaiman, N. Nelson, Structure and function of wild-type and subunit-depleted photosystem I in Synechocystis, Biochim. Biophys. Acta Bioenerg. 1859 (2018) 645–654, https://doi.org/10.1016/j.bbabio.2018.02.002.
[7] C. Gisriel, G. Shen, V. Kurashov, M. Ho, S. Zhang, D. Williams, J.H. Golbeck, P. Fromme, D.A. Bryant, The structure of Photosystem I acclimated to far-red light illuminates an ecologically important acclimation process in photosynthesis, Sci. Adv. 6 (2020) eaay6415. doi:https://doi.org/10.1126/sciadv.aay6415.
[8] R. Croce, H. van Amerongen, Natural strategies for photosynthetic light harvesting, Nat. Chem. Biol. 10 (2014) 492–501, https://doi.org/10.1038/nchembio.1555.
[9] J.H. Golbeck (Ed.), Photosystem I: The Light-driven Plastocyanin: Ferredoxin Oxidoreductase, Springer Netherlands, Dordrecht, 2006, , https://doi.org/10.1007/978-1-4020-4256-0.
[10] N. Nelson, Plant photosystem I – the most efficient nano-photochemical machine, J. Nanosci. Nanotechnol. 9 (2009) 1709–1713, https://doi.org/10.1166/jnn.2009.SI01.
[11] R. Croce, H. van Amerongen, Light-harvesting in photosystem i, Photosynth. Res. 116 (2013) 153–166, https://doi.org/10.1007/s11120-013-9838-x.
[12] V. Kurashov, M.-Y. Ho, G. Shen, K. Piedl, T.N. Laremore, D.A. Bryant, J.H. Golbeck, Energy transfer from chlorophyll f to the trapping center in naturally occurring and engineered Photosystem I complexes, Photosynth. Res. 141 (2019) 151–163, https://doi.org/10.1007/s11120-019-00616-x.
[13] L.O. Björn, G.C. Papageorgiou, R.E. Blankenship, Govindjee, a viewpoint: why chlorophyll a? Photosynth. Res. 99 (2009) 85–98, https://doi.org/10.1007/s11120-008-9395-x.
[14] H. Dau, I. Zaharieva, Principles, efficiency, and blueprint character of solar-energy conversion in photosynthetic water oxidation, Acc. Chem. Res. 42 (2009) 1861–1870, https://doi.org/10.1021/ar900225y.
[15] A.W. Rutherford, A. Osyczka, F. Rappaport, Back-reactions, short-circuits, leaks and other energy wasteful reactions in biological electron transfer: redox tuning to survive life in O 2, FEBS Lett. 586 (2012) 603–616, https://doi.org/10.1016/j.febslet.2011.12.039.
[16] H. Miyashita, H. Ikemoto, N. Kurano, K. Adachi, M. Chihara, S. Miyachi, Chlorophyll d as a major pigment, Nature 383 (1996) 402, https://doi.org/10.1038/383402a0.
[17] P. Loughlin, Y. Lin, M. Chen, Chlorophyll d and Acaryochloris marina: current status, Photosynth. Res. 116 (2013) 277–293, https://doi.org/10.1007/s11120-013-9829-y.
[18] H. Miyashita, Discovery of chlorophyll d in Acaryochloris marina and chlorophyll f in a unicellular Cyanobacterium, strain KC1, isolated from Lake Biwa, J. Phys. Chem. Biophys. 4 (2014) 1–9, https://doi.org/10.4172/2161-0398.1000149.
[19] M. Chen, M. Schliep, R.D. Willows, Z.-L. Cai, B.A. Neilan, H. Scheer, A red-shifted chlorophyll, Science (80-.). 329 (2010) 1318–1319. doi:https://doi.org/10.1126/science.1191127.
[20] Y. Li, Z. Cai, M. Chen, Spectroscopic properties of chlorophyll f, J. Phys. Chem. B 117 (2013) 11309–11317, https://doi.org/10.1021/jp402413d.
[21] M.-Y. Ho, G. Shen, D.P. Canniffe, C. Zhao, D.A. Bryant, Light-dependent chlorophyll f synthase is a highly divergent paralog of PsbA of photosystem II, Science (80-.). 353 (2016) aaf9178–aaf9178. doi:https://doi.org/10.1126/science.aaf9178.
[22] F. Gan, D.A. Bryant, Adaptive and acclimative responses of cyanobacteria to far-red light, Environ. Microbiol. 17 (2015) 3450–3465, https://doi.org/10.1111/1462-2920.12992.
[23] F. Gan, S. Zhang, N.C. Rockwell, S.S. Martin, J.C. Lagarias, D.A. Bryant, Extensive remodeling of a cyanobacterial photosynthetic apparatus in far-red light, Science (80-.). 345 (2014) 1312–1317. doi:https://doi.org/10.1126/science.1256963.
[24] F. Gan, G. Shen, D.A. Bryant, Occurrence of far-red light photoacclimation (FaRLiP) in diverse cyanobacteria, Life 5 (2014) 4–24, https://doi.org/10.3390/life5010004.
[25] D.J. Nürnberg, J. Morton, S. Santabarbara, A. Telfer, P. Joliot, L.A. Antonaru, A. V. Ruban, T. Cardona, E. Krausz, A. Boussac, A. Fantuzzi, A.W. Rutherford, A. William Rutherford, Photochemistry beyond the red limit in chlorophyll f–containing photosystems, Science (80-.). 360 (2018) 1210–1213. doi:https://doi.org/10.1126/science.aar8313.
[26] M.-Y. Ho, D.M. Niedzwiedzki, C. MacGregor-Chatwin, G. Gerstenecker, C.N. Hunter, R.E. Blankenship, D.A. Bryant, Extensive remodeling of the photosynthetic apparatus alters energy transfer among photosynthetic complexes when cyanobacteria acclimate to far-red light, Biochim. Biophys. Acta - Bioenerg. (2019) 148064. doi:https://doi.org/10.1016/j.bbabio.2019.148064.
[27] W.M. Manning, H.H. Strain, W.M. Manning, Chlorophyll d, a green pigment of red algae, J. Biol. Chem. 151 (1943) 1–19 http://www.jbc.org/cgi/content/short/151/1/1 , Accessed date: 28 August 2019.
[28] M. Chen, Y. Li, D. Birch, R.D. Willows, A cyanobacterium that contains chlorophyll f - a red-absorbing photopigment, FEBS Lett. 586 (2012) 3249–3254, https://doi.org/10.1016/j.febslet.2012.06.045.
[29] M. Chen, R.E. Blankenship, Expanding the solar spectrum used by photosynthesis, Trends Plant Sci. 16 (2011) 427–431, https://doi.org/10.1016/j.tplants.2011.03.011.
[30] R.E. Blankenship, M. Chen, Spectral expansion and antenna reduction can enhance photosynthesis for energy production, Curr. Opin. Chem. Biol. 17 (2013) 457–461, https://doi.org/10.1016/j.cbpa.2013.03.031.
[31] D.R. Ort, S.S. Merchant, J. Alric, A. Barkan, R.E. Blankenship, R. Bock, R. Croce, M.R. Hanson, J.M. Hibberd, S.P. Long, T.A. Moore, J. Moroney, K.K. Niyogi, M.A.J. Parry, P.P. Peralta-Yahya, R.C. Prince, K.E. Redding, M.H. Spalding, K.J. van Wijk, W.F.J. Vermaas, S. von Caemmerer, A.P.M. Weber, T.O. Yeates, J.S. Yuan, X.G. Zhu, Redesigning photosynthesis to sustainably meet global food and bioenergy demand, Proc. Natl. Acad. Sci. 112 (2015) 8529–8536, https://doi.org/10.1073/pnas.1424031112.
[32] X.-G.G. Zhu, Q. Song, D.R. Ort, Elements of a dynamic systems model of canopy photosynthesis, Curr. Opin. Plant Biol. 15 (2012) 237–244, https://doi.org/10.1016/j.pbi.2012.01.010.
[33] A. Rivadossi, G. Zucchelli, F.M. Garlaschi, R.C. Jennings, The importance of PSI

chlorophyll red forms in light-harvesting by leaves, Photosynth. Res. 60 (1999) 209–215, https://doi.org/10.1023/A:1006236829711.
[34] S.P. Mielke, N.Y. Kiang, R.E. Blankenship, M.R. Gunner, D. Mauzerall, Efficiency of photosynthesis in a Chl d-utilizing cyanobacterium is comparable to or higher than that in Chl a-utilizing oxygenic species, Biochim. Biophys. Acta Bioenerg. 1807 (2011) 1231–1236, https://doi.org/10.1016/j.bbabio.2011.06.007.
[35] G. Shen, D.P. Canniffe, M.-Y. Ho, V. Kurashov, A. van der Est, J.H. Golbeck, D.A. Bryant, Characterization of chlorophyll f synthase heterologously produced in Synechococcus sp. PCC 7002, Photosynth. Res. 140 (2019) 77–92. doi:https://doi.org/10.1007/s11120-018-00610-9.
[36] M. Ludwig, D.A. Bryant, Transcription profiling of the model cyanobacterium Synechococcus sp. strain PCC 7002 by next-gen (SOLiD™) sequencing of cDNA, Front. Microbiol. 2 (2011) 1–23. doi:https://doi.org/10.3389/fmicb.2011.00041.
[37] D.H. Lambert, S.E. Stevens, Photoheterotrophic growth of Agmenellum quadruplicatum PR-6, J. Bacteriol. 165 (1986) 654–656, https://doi.org/10.1128/jb.165.2.654-656.1986.
[38] G. Shen, J. Zhao, S.K. Reimer, M.L. Antonkine, Q. Cai, S.M. Weiland, J.H. Golbeck, D.A. Bryant, Assembly of photosystem I: I. Inactivation of the rubA gene encoding a membrane-associated rubredoxin in the cyanobacterium Synechococcus sp. PCC 7002 causes a loss of photosystem I activity, J. Biol. Chem. 277 (2002) 20343–20354. doi:https://doi.org/10.1074/jbc.M201103200.
[39] G. Shen, F. Gan, D.A. Bryant, The siderophilic cyanobacterium Leptolyngbya sp. strain JSC-1 acclimates to iron starvation by expressing multiple isiA-family genes, Photosynth. Res. 128 (2016) 325–340. doi:https://doi.org/10.1007/s11120-016-0257-7.
[40] T. Malavath, I. Caspy, S.Y. Netzer-El, D. Klaiman, N. Nelson, Structure and function of wild-type and subunit-depleted photosystem I in Synechocystis, Biochim. Biophys. Acta Bioenerg. 1859 (2018) 645–654, https://doi.org/10.1016/j.bbabio.2018.02.002.
[41] C. Le Quiniou, L. Tian, B. Drop, E. Wientjes, I.H.M. van Stokkum, B. van Oort, R. Croce, PSI–LHCI of Chlamydomonas reinhardtii: increasing the absorption cross section without losing efficiency, Biochim. Biophys. Acta Bioenerg. 1847 (2015) 458–467, https://doi.org/10.1016/j.bbabio.2015.02.001.
[42] J.J. Snellenburg, S.P. Laptenok, R. Seger, K.M. Mullen, I.H.M. van Stokkum, Glotaran: A Java-based graphical user interface for the R package TIMP, J. Stat. Softw. 49 (2012) 1–22. doi:10.18637/jss.v049.i03.
[43] I.H.M. van Stokkum, D.S. Larsen, R. van Grondelle, Global and target analysis of time-resolved spectra, Biochim. Biophys. Acta Bioenerg. 1657 (2004) 82–104, https://doi.org/10.1016/j.bbabio.2004.04.011.
[44] J.J. Snellenburg, J.P. Dekker, R. van Grondelle, I.H.M. van Stokkum, Functional compartmental modeling of the photosystems in the thylakoid membrane at 77 K, J. Phys. Chem. B 117 (2013) 11363–11371, https://doi.org/10.1021/jp4031283.
[45] N. V. Karapetyan, E. Schlodder, R. van Grondelle, J.P. Dekker, The long wavelength chlorophylls of Photosystem I, in: Photosyst. I, Springer Netherlands, Dordrecht, 2006: pp. 177–192. doi:https://doi.org/10.1007/978-1-4020-4256-0_13.
[46] B. Gobets, I.H.M. van Stokkum, M. Rögner, J. Kruip, E. Schlodder, N.V. Karapetyan, J.P. Dekker, R. van Grondelle, Time-resolved fluorescence emission measurements of Photosystem I particles of various cyanobacteria: a unified compartmental model, Biophys. J. 81 (2001) 407–424, https://doi.org/10.1016/S0006-3495(01)75709-8.
[47] I.H.M. Van Stokkum, T.E. Desquilbet, C.D. Van Der Weij-De Wit, J.J. Snellenburg, R. Van Grondelle, J.C. Thomas, J.P. Dekker, B. Robert, Energy transfer and trapping in red-chlorophyll-free photosystem i from Synechococcus WH 7803, J. Phys. Chem. B 117 (2013) 11176–11183, https://doi.org/10.1021/jp401364a.
[48] D.M. Niedzwiedzki, H. Liu, M. Chen, R.E. Blankenship, Excited state properties of chlorophyll f in organic solvents at ambient and cryogenic temperatures, Photosynth. Res. 121 (2014) 25–34, https://doi.org/10.1007/s11120-014-9981-z.
[49] Y. Li, N. Scales, R.E. Blankenship, R.D. Willows, M. Chen, Extinction coefficient for red-shifted chlorophylls: chlorophyll d and chlorophyll f, Biochim. Biophys. Acta Bioenerg. 1817 (2012) 1292–1298, https://doi.org/10.1016/j.bbabio.2012.02.026.
[50] B. Gobets, I.H.M. van Stokkum, F. van Mourik, J.P. Dekker, R. van Grondelle, Excitation wavelength dependence of the fluorescence kinetics in Photosystem I particles from Synechocystis PCC 6803 and Synechococcus elongatus, Biophys. J. 85 (2003) 3883–3898, https://doi.org/10.1016/S0006-3495(03)74803-6.
[51] C. Le Quiniou, Influence of Size, Composition and Supramolecular Organization of Photosystem I on Trapping Efficiency: Insights From the Algae Chlamydomonas Reinhardtii and Nannochloropsis Gaditana, Vrije Universiteit Amsterdam, 2016.
[52] M. Brecht, J.B. Nieder, H. Studier, E. Schlodder, R. Bittl, Red antenna states of photosystem I from Synechococcus sp. PCC 7002, Photosynth. Res. 95 (2008) 155–162. doi:https://doi.org/10.1007/s11120-007-9241-6.
[53] C. Slavov, E. El-Mohsnawy, M. Rögner, A.R. Holzwarth, Trapping kinetics in isolated cyanobacterial PS I complexes, Chem. Phys. 357 (2009) 163–170, https://doi.org/10.1016/j.chemphys.2008.12.021.
[54] R.E. Blankenship, Molecular Mechanisms of Photosynthesis, Blackwell Science, Oxford, 2002https://www.wiley.com/en-us/Molecular+Mechanisms+of+Photosynthesis-p-9780470758472.